# DNS OF TURBULENT CHANNEL FLOW WITH A ELASTIC CANTILEVER

**Koichi TSUJIMOTO**
Division of Mechanical Engineering
Graduate School of Engineering, Mie University
1577 Kurimamachiya-cho, Tsu, 514-8507 Japan
tujimoto@mach.mie-u.ac.jp

**Yasunori SASAKI, Toshihiko SHAKOUCHI and Toshitake ANDO**
Division of Mechanical Engineering
Graduate School of Engineering, Mie University
1577 Kurimamachiya-cho, Tsu, 514-8507 Japan

## ABSTRACT

Numerical solving of fluid-structure interaction (FSI) problems are of importance in various scientific fields. In particular, the establishment of stable numerical scheme is needed in order to analyze the details of flow phenomena. In the present paper, we propose a weak-coupling method for FSI problem: for a elastic body the rigorous equations of motion are discretized with finite volume method; in the flow computation, the elastic body object is reproduced via immersed boundary method. To demonstrate the performance of proposed scheme, the 3D structure analysis and 3D FSI problems of a elastic body are solved. The results indicate that the computation is stably conducted using the proposed method, in spite of the occurrence of fairly large deformation of the object. In addition it turns out that the realistic flow including turbulence phenomena is well reproduce using the proposed FSI scheme.

## Introduction

Fluid-Structure Interaction (FSI) problem is concerned with in various research fields such as mechanical, aerospace, civil and medical engineering. The highly accurate and stable scheme for the FSI problem is desired to be developed. In the view of numerical difficulty, while the FSI for the structure of rigid body is easiest problem, the large deformation of structure often induces the divergence of computation due to the distorted grid. Namely depending on the rate of deformation, the treatment of FSI problem is difficult. In general, the major numerical method for FSI problem is divide into two category, *i.e.*, strong-coupling method (Zhang et al., 2001) or monolithic method (Huber et al., 2004; Blom et al., 1998) and weak-coupling method (Piperno et al., 1997; Farhat et al., 2000). As the merit of strong coupling it has been already mentioned that the governing equations of both fluid and structure are simultaneously solved, resulting in the stable and high-accurate computation. On the other hand in the weak-coupling method, since the both computation of fluid and structure are performed independently of each other, the performance for the stability and accuracy is inferior than that of strong-coupling. However, the conventional code for the structure and flow computation can be utilized through the slightly modification in which the information is alternatively exchange between flow and structure. Recently, since IB method (Peskin, 1981; Fadlun et al.,2000) in the flow computation is capable of dealing with any moving structures, a keen issue needing to be solved in the FSI problem including the large deformation structures, concentrates to the development of the stable structure computation. In the present study, we pay attention to develop the stable scheme for structure computation, and propose the weak-coupling method in which for the elastic body the rigorous equations of motion are discretized with finite volume method (FVM); for the flow computation, the finite difference method (FDM)is used and the elastic body is reproduced via immersed boundary method (Fadlun et al.,2000). Using the proposed scheme, DNS of turbulent channel flow with a elastic cantilever is conducted. The modification of turbulent flow due to the elastic motion is demonstrated through the visualization of instantaneous and time-averaged mean flow fields.

## Finite volume method for elastic body

The dynamics of elastic body based on the continuum model can be written by the conservation law of mass and momentum:

$$\frac{d\rho}{dt} = -\rho \frac{\partial u_i}{\partial x_i} \tag{1}$$

$$\rho \frac{du_i}{dt} = \frac{\partial \sigma_{ij}}{\partial x_j} \tag{2}$$

where $\rho$ is the density, $u_i$ is velocity component

In the present study, constitutive equations are assumed to be a Hookean elastic body:

$$\sigma_{ij} = s_{ij} - p\delta_{ij} - q_{ij} \tag{3}$$

$$\frac{d^J s_{ij}}{dt} = G(\dot{\varepsilon}_{ij} - \frac{1}{3} tr\,(\dot{\varepsilon})\,\delta_{ij}) \tag{4}$$

$$\dot{\varepsilon}_{ij} = \left(\frac{\partial u_i}{\partial x_j} + \frac{\partial u_j}{\partial x_i}\right) \tag{5}$$

$$\frac{dp}{dt} = -K\,tr(\dot{\varepsilon}) \tag{6}$$

where $s_{ij}$ is the stress deviator tensor$\varepsilon_{ij}$ strain tensor and $\dot{\varepsilon}_{ij}$ the rate of strain. $G$ is the modulus of elasticity $K$ the bulk modulus $q_{ij}$ artificial viscosity tensor and $p$ pressure. $tr(\dot{\varepsilon})$ is the trace of the tensor $\dot{\varepsilon}$:

$$tr\,(\dot{\varepsilon}) = \left(\frac{\partial u_i}{\partial x_i} + \frac{\partial u_j}{\partial x_j} + \frac{\partial u_k}{\partial x_k}\right) \tag{7}$$

G and K are written by the Young's modulus $E$ and the Poisson ratio $\gamma$:

$$G = \frac{E}{2(1+\gamma)}, K = \frac{E}{3(1-2\gamma)} \tag{8}$$

In order to consider the large deformation of elastic body, the rate of stress $\frac{d^J s_{ij}}{dt}$ is introduced. $\frac{d^J s_{ij}}{dt}$ is called as the Jaumann derivative which means the rate of stress tensor in a reference frame being corrected according to the rotational effect:

$$\frac{d^J s_{ij}}{dt} = \dot{s}_{ij} + s_{ik}\Omega_{kj} + s_{kj}\Omega_{ik} \tag{9}$$

where $\Omega_{ij}$ is an antisymetric rotation tensor:

$$\Omega_{ij} = \left(\frac{\partial u_j}{\partial x_i} - \frac{\partial u_i}{\partial x_j}\right) \tag{10}$$

The governing equations are discretized using the hexahedron element proposed in a classical FVM (Mark,2006). The velocity and the displacement are defined at the grid points constructing the hexahedron element, and the stress is at the center of the element. The temporal discretization is as follows (Mark, 2006);

$$\varepsilon_{ij}^{n+1/2} = \left[\left(\frac{\partial u_i}{\partial x_j}\right)^{n+1/2} + \left(\frac{\partial u_j}{\partial x_i}\right)^{n+1/2}\right]\Delta t \tag{11}$$

$$s_{ij}^{n+1} = s_{ij}^n + G\left[\varepsilon_{ij}^{n+1/2} - \frac{1}{3} tr\left(\dot{\varepsilon}^{n+1/2}\right)\delta_{ij}\right]\Delta t - \left[s_{ik}^n \Omega_{kj}^n + s_{kj}^n \Omega_{ik}^n\right]\Delta t \tag{12}$$

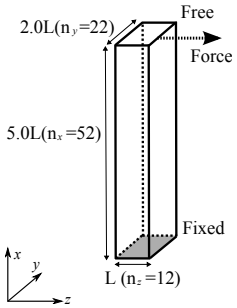


Figure 1. Computational domain and coordinate system of a cantilever

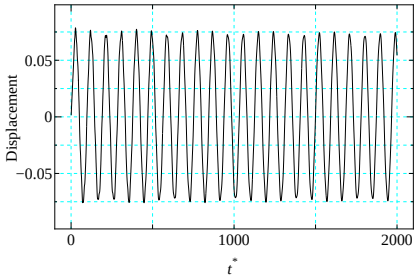


Figure 2. Time evolution of tip displacement for the free-vibrating cantilever

$$u_i^{n+1/2} = u_i^{n-1/2} + \left(\frac{du}{dt}\right)_i^n \Delta t \tag{13}$$

$$x_i^{n+1} = x_i^n + u_i^{n+1/2}\Delta t \tag{14}$$

$$x_i^{n+1/2} = \frac{1}{2}(x_i^{n+1} + x_i^n) \tag{15}$$

## Dynamic of three-dimensional cantilever

In order to evaluate the validation of simulation code, vibration analysis of a fixed-free cantilever is examined. In the present study, the shape of cantilever is shown in Fig.1. The dimension of cantilever is $5L \times 2L \times L$, and the grid size is $n_x \times n_y \times n_z = 52 \times 22 \times 12$. The end of cantilever is fixed at $x = 0$ and the another end is free. The free end of cantilever is displaced $1/20L$ in $z$ direction at initial instant, and then the cantilever continues to freely oscillate. Figure 2 shows the time evolution of the tip displacement of cantilever in $z$ direction. Since the Hookean elastic model is assumed, the amplitude of oscillation is constant as well as the periods of oscillation. Table 1 shows the comparison of the theoretical value and the present results as for the natural frequency The theoretical value, $f_T^*$ is as follows (Harris, 1961):

$$f_T^* = \frac{\lambda}{2\pi}\frac{1}{L^2}\sqrt{\frac{EI}{\rho A}} \tag{16}$$

$\rho$; density ,$E$; Young's modulus
$I$; moment of inertia in the plane or second moment of area
$L$; length of cantilever
$A$; cross sectional area of cantilever $\lambda$; Eigen value

Table 1. Comparison of computational value with theoretical value

| | Frequency | Error |
|---|---|---|
| Theoretical Value | 0.01110 | - |
| Computational value | 0.01070 | 3.8% |

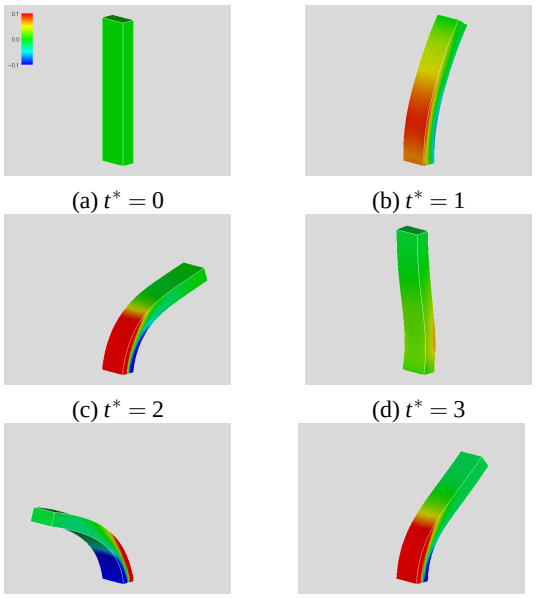

(a) $t^* = 0$ (b) $t^* = 1$ (c) $t^* = 2$ (d) $t^* = 3$ (e) $t^* = 4$ (f) $t^* = 5$

Figure 3. Contours of normal stress $\sigma_{xx}$ of the large-deformed cantilever

In this calculation, $\lambda$ = 3.52 is selected as the first bending mode (Harris, 1961). From Table 1, the computational results are good agreement with the theoretical value suggesting the computational code is established. In order to investigate whether the improved FVM scheme is able to reproduce the behavior of large deformation, the cantilever is deformed by adding the strong external force. As the test case, previous mentioned cantilever shown in Fig.1 is deformed by a strong force adding at the free end of cantilever. Figures 3 show the surface distribution of normal stress $\sigma_{xx}$. In the figures, the red and blue color correspond to the tensile and the compression stress, respectively. When the large deformation occurs in Fig.3(c), the strong stress distribute around the root of cantilever, demonstrating that the fairly large deformation are reproduced through the stable computation.the.

## Numerical scheme for FSI problem

In the present study, we propose the weak-coupling method for FSI. therefore the numerical scheme should be prepared for each of structure and flow field. For the flow computation, the governing equation for unsteady incompressible viscous flow in Cartesian coordinates system are as

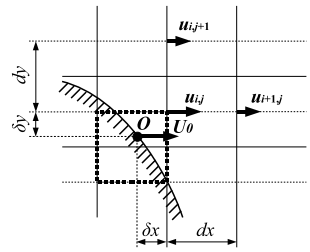


Figure 4. Schematic of interpolation scheme for velocity

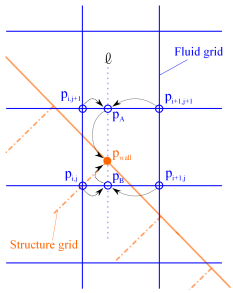


Figure 5. Schematic of interpolation scheme for pressure

follows:

$$\frac{\partial u_i}{\partial x_i} = 0 \tag{17}$$

$$\frac{\partial u_i}{\partial t} + \frac{\partial u_i u_j}{\partial x_j} = -\frac{1}{\rho}\frac{\partial p}{\partial x_i} + \frac{1}{Re}\frac{\partial^2 u_i}{\partial x_j \partial x_j} \tag{18}$$

where, $Re$ is Reynolds number. The momentum equations are discretized using the Crank-Nicolson method for the viscous term and the second-order Adams-Bashforth method for convective terms. The discretization is performed with the fractional-step method (Kim et al., 1985):

$$\frac{\hat{u}_i - u_i^n}{\Delta t} = \frac{3}{2}H_i^n - \frac{1}{2}H_i^{n-1} - \nabla p^n + \frac{1}{2Re}\nabla^2(\hat{u}_i + u_i^n) \tag{19}$$

where the superscript 'n' means the index of time step and $\hat{u}_i$ is the intermediate velocity component. $H_i$ represents the convective terms

Introducing $\Delta\hat{u}_i = \hat{u}_i - u_i^n$, the momentum equations can be written as:

$$\left(1 - \frac{\Delta t}{2Re}\nabla^2\right)\Delta\hat{u}_i = \Delta t\left\{\frac{3}{2}H_i^n - \frac{1}{2}H_i^{n-1} - \nabla p^n + \frac{1}{Re}\nabla^2 u_i^n\right\} \tag{20}$$

To satisfy the continuity equation, $\nabla \cdot u_i^{n+1} = 0$ should be established. thus

$$\nabla \cdot \left(\nabla\phi^{n+1}\right) = \frac{1}{\Delta t}\nabla \cdot \hat{u}_i \tag{21}$$

$$u_i^{n+1} = \hat{u}_i - \Delta t \nabla \phi^{n+1} \tag{22}$$

$$p^{n+1} = p^n + \phi^{n+1} - \frac{\Delta t}{2Re}\nabla^2\phi^{n+1} \tag{23}$$

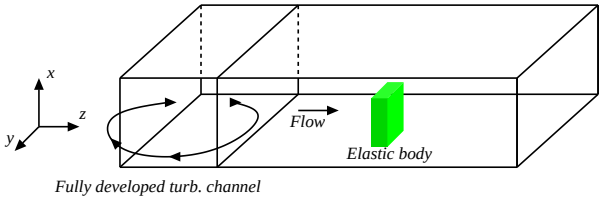


Figure 6. Computational domain of a channel flow

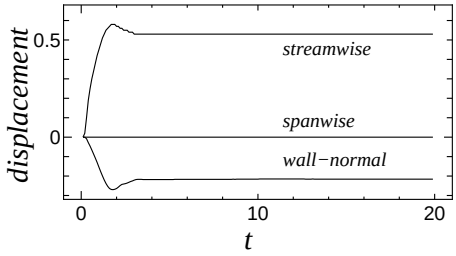


Figure 7. Time evolution of tip displacement of the elastic cantilever in the uniform inflow.

Th spatial discretization is performed with a second-order central difference scheme. The staggered grid system is employed. In the flow computation, the interface between fluid and structure is tracked using immersed boundary(IB) method. In the IB method, to represent the boundary on the Eulerian grid, the external force is imposed at the boundary in the flow field so that the boundary velocity is a specified value. The original concept was proposed by Paskin (1981). However, it is well-known the shortcoming, in which the time step should be considerable small compared to the usual one being decided by a CFL condition (Fadlun et al., 2000). To avoid this problem, Fadlun et al. (2000) proposed the improved IB method called as 'Direct forcing method'. In the present study, in order to easily express an object of arbitrarily shape, the material point is introduced. As shown Fig.4, for the two-dimensional problem, the velocity at the grid point in the vicinity of the wall, $u_{ij}$ is approximated with both the wall velocity, $U_o$ and the velocity at the slightly distance from the wall, $u_{i+1,j}$and $u_{i,j+1}$.Thus the relation between these points is as follows:

$$u_{i,j}^{n+1} = aU_{\mathrm{O}} + bu_{i+1,j}^{n+1} + c_{i,j+1}^{n+1} \tag{24}$$

where the coefficients are geometrically-determined.

$$a = \frac{1}{\frac{dx-\delta x}{dx} + \frac{dy-\delta y}{dy} + 1}$$
$$b = \frac{\frac{dx-\delta x}{dx}}{\frac{dx-\delta x}{dx} + \frac{dy-\delta y}{dy} + 1}$$
$$c = \frac{\frac{dy-\delta y}{dy}}{\frac{dx-\delta x}{dx} + \frac{dy-\delta y}{dy} + 1}$$

The approximated relation obtained for the intermediate velocity,

$$\Delta\hat{u}_{i,j} - b\Delta\hat{u}_{i+1,j} - c\Delta\hat{u}_{i,j+1} = aU_{\mathrm{O}} - u_{i,j}^{n} + bu_{i+1,j}^{n} + cu_{i,j+1}^{n} \tag{25}$$

is incorporated into the implicit treatment of viscous diffusion term (Fadlun et al., 2000).

As shown in Fig.5, the pressure at the structure grid, $p_{wall}$ is linearly interpolated from the pressure at the fluid computational grid located around the structure grid. For the structure computation, the external force is estimated using $P_{wall}$. The above-mentioned procedure is summarized as follows:

1. The flow computation is conducted using finite difference method to satisfy the interface boundary condition using IB method (Fig.4).
2. The pressure at the interface obtained from flow computation is interpolated from the flow field to the structure grid (Fig.5).
3. The structure computation is conducted using finite volume method to satisfy the interface boundary condition.

Through the step $1 \sim 3$ are sequentially repeated, FSI problem will be solved

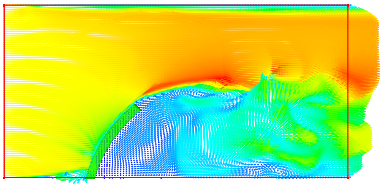

(a) Velocity vector plots in $x-z$ plane

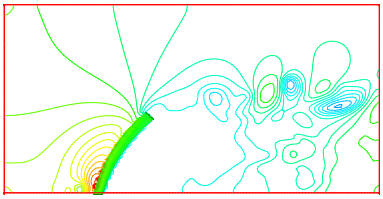

(b) Contour of pressure in $x-z$ plane

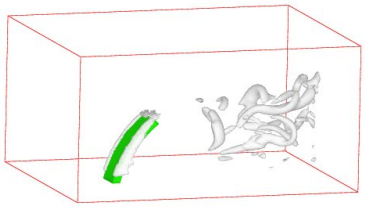

(c) Iso-surface of Q criteria

Figure 8. Instantaneous flow field around the elastic cantilever in a uniform flow.

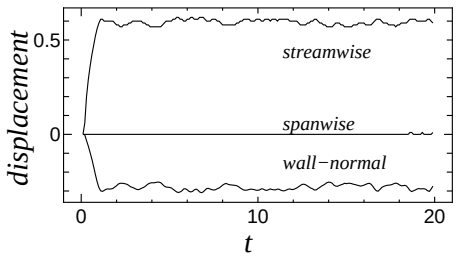


Figure 9. Time evolution of the tip displacement of elastic cantilever in the turbulent channel low.

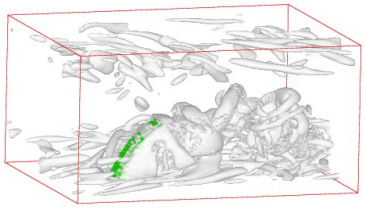

(a) elastic

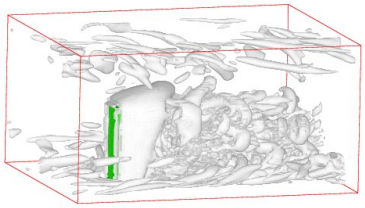

(b) rigid

Figure 10. Isosurface of Q criteria in a fully-developed turbulent flow.

## FSI for three-dimensional problem

The computational volume is embedded with two-parallel walls shown in Fig.6. The wall condition is enforced on the both upper and lower boundary. The cantilever is placed on the lower boundary. As inflow conditions, laminar and turbulent flow are examined. As the laminar flow, a uniform flow $U_0$ is imposed on the left side boundary and a convective outflow boundary is used on the right side boundary. Periodicity is enforced in spanwise direction. The grid size is $n_x \times n_y \times n_z = 128 \times 80 \times 128$ in $x$, $y$ and $z$ directions. The dimension of computational domain is $H_x \times H_y \times H_z = 2L \times 3.14L \times 4L$. The Reynolds number is $Re = U_0 L/\nu = 3000$. As the fully-developed turbulent inflow, a computation of turbulent channel flow having its computational volume, 2.0L×3.14L×6.28 and its grid number, $n_x \times n_y \times n_z = 128 \times 128 \times 100$ is conducted. The Reynolds number defined with the friction velocity,$w_\tau \left(= \sqrt{\nu \frac{\partial w}{\partial y}|_{y=0}}\right)$ is $Re_\tau = (w_\tau h/\nu) = 150$. The cantilever is equipped at the distance $0.25H_z$ from inlet, and its dimension is $L \times 0.4L \times 0.1L$ and its grid number, $52 \times 22 \times 10$.

## Dynamics of a cantilever in a uniform flow

Figure 7 shows the time evolution of tip displacement of the elastic cantilever. After the start of simulation, the cantilever continues to deform until $t \approx 3$, and then maintains the deformed profile without the oscillation. Also the spanwise deformation does not occur at all.

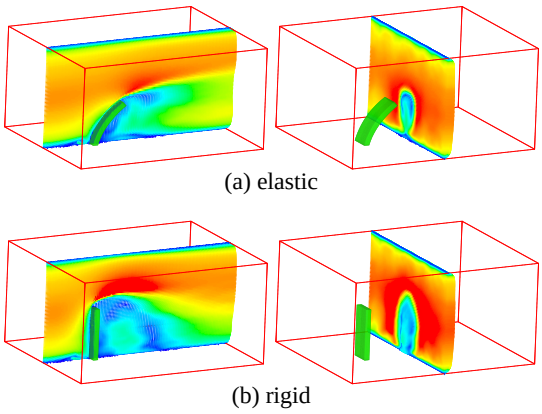

(a) elastic

(b) rigid

Figure 11. Vector plots of mean velocity (left:in $x-z$ plane; right: in $x-y$ plane)

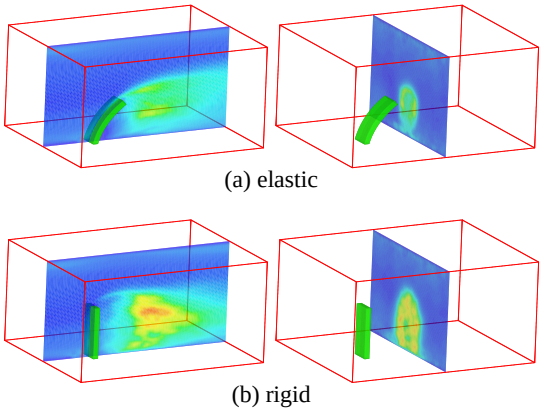

(a) elastic

(b) rigid

Figure 12. Contour of turbulent kinetic energy (left:in $x-z$ plane; right: in $x-y$ plane)

Figures 8 show the instantaneous flow field around the elastic cantilever. From Fig.8(a)(b), the flow along the surface of cantilever and the large-scale recirculation behind the cantilever are found; the contour lines of pressure penetrate normal to the surface of cantilever, suggesting that the IB method well represents the shape of cantilever. Figure 8(c) shows the isosurfaces of the second invariance of velocity gradient tensor, Q criteria which identifies vortical structures. The vortical structures (gray color) extends on the strong shear around the corner of cantilever, and the tube-like structures are generated further downstream.

## Dynamics of cantilevers in a fully developed turbulent flow

In order to investigate effects of elasticity, a rigid or elastic cantilever is placed in the turbulent channel flow. Figure 9 shows the time evolution of tip displacement of the elastic cantilever. As well as the uniform inflow condition, after the start of simulation, the cantilever continues to deform without

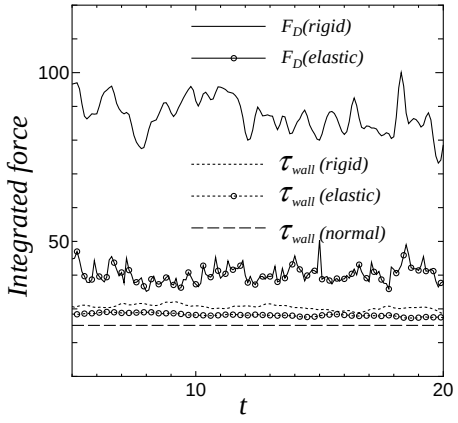


Figure 13. Time evolution of drag force

the spanwsie deformation. However, differently to that of uniform flow, the cantilever oscillates with no definite frequency.

Figures 10 show the instantaneous view of vortical structures around the cantilever. The flow phenomena in which quasi-streamwise vortices over the upper wall are formed, are exactly the same in both cases suggesting that the usual near-wall turbulence structures of channel flow are maintained upper wall. For the rigid case, a large number of fine-scale vortices are formed in the wake of cantilever, while for the elastic case the existence of hairpin vortices can be found.

Figures 11 show vector plots of mean flow velocity averaged in $t = 5 \sim 20$. In the Fig. the color means the magnitude of velocity vector. In both figures, the high speed region extends over the cantilever because of the contraction due to the cantilever, and the recirculation region behind the cantilever are formed. The dimension of the wake of the elastic case shrinks due to the deformation than that of rigid case. Figures 12 show contour of turbulent kinetic energy. Although the peaks of TKE appears at the vicinity of the wall of the usual-turbulent channel, the TKE of the current cases markedly is enhanced in the wake.

The drag of cantilever, $F_D$ is approximated using the streamwise momentum equation.

$$F_D \approx -\int\int \left[ww + \frac{1}{\rho}p - \nu\frac{\partial w}{\partial z}\right]_{z=0}^{z=Hz} dxdy + \int\int \frac{1}{\rho}\left[\tau_{wall}\right]_{x=0}^{x=Hx} dydz \qquad (26)$$

Figure 13 shows the time evolution of wall-shear stress, $\tau_{wall}$ and the drag of cantilever including both the profile and friction drag, $F_D$. Compared to the wall-shear stress of the usual channel (as indicated by broken line), a large increase in the present results does not occur, and the difference of wall-shear between the rigid and the elastic case is a little, while the drag of cantilever is largely different between both cases. Although the projected area of elastic cantilever to the flow reduces about 70 percent of rigid cases, the drag reduction of the elastic case to the rigid one is about 50 percent. The reason of this finding is that the large deformation of elastic cantilever induces the shrinking of the wake region.

## Conclusions

We propose the weak coupling method: FVM for the structure computation, FDM for the flow computation and both scheme are connected by IB method. The large- deformed elastic body are simulated using the proposed scheme. Conclusions are as follows:

1. The classical FVM is capable of stably simulating the large deformation of structures; the flow induced by the large deformation of elastic cantilever is reproduced by IB method in the flow computation. Thus we confirm that the proposed weak-coupling method is useful for the FSI problem.
2. The FSI problem between turbulent field and elastic body is stably solved, demonstrating that the proposed scheme is capable of treating the three-dimensional realistic flow, in addition it is found that the peculiar flow phenomena induced by the large-deformation of elastic body appears.

## REFERENCES


Blom, F., 1998, "A monolithical fluid-structure interaction algorithm applied to the piston problem", Comput. Methods Appl. Mech. Eng. Vol. 167, pp.369-391.

Fadlun, E. A., Verzicco, R., Orlandi, P., and Yusof, J. M., 2000, "Combined Immersed-Boundary Finite-Difference Methods for Three-Dimensional Complex Flow Simulations", J. Comp. Physics, Vol. 161, pp. 35-60.

Farhat, C., and Lesoinne, M., 2000, "Two efficient staggered algorithms for the serial and parallel solution of three-dimensional nonlinear transient aeroelastic problems", Comp. Meth. Appl. Mech. Eng., Vol. 182, pp. 499-515.

Harris, C. M., 1961, "Shock and Vibration Handbook", Mcgraw-Hill Handbooks.

Hubner, B., Walhorn, E., and Dinkler, D. A., 2004, Monolithic approach to fluid-structure interaction using space-time finite elements, Comput. Meth. Appl. Mech. Eng. Vol. 193, pp. 2087-2104.

Kim, J., and Moin, P., 1985, "Application of a fractional step method to incompressible flows", J. Comp. Physics, Vol. 59, pp. 308-323.

Piperno, S., 1997, "Explicit/implicit fluid/structure staggered procedures with a structural predictor and fluid subcycling for 2D inviscid aeroelastic simulations", Int. J. Num. Meth. Fluids, Vol. 25, pp. 1207-1226.

Peskin, C. S. , 1981, "The fluid dynamics of heart valves: Experi- mental, theoretical and computational methods", Ann. Rev. Fluid Mech. Vol. 14, pp. 235-259.

Wilkins, M. L., 2006, "Computer Simulation of Dynamic Phenomena", Springer Verlag GmbH.

Zhang, Q., and Hisada,T., 2001,"Analysis of fluid-structure interaction problems with structural buckling and large domain changes by. ALE finite element method", Comput. Methods Appl. Mech. Eng., Vol. 190, pp. 6341-6357.